ADVANCED MATERIALS TECHNOLOGIES
www.advmattechnol.de

Event-Driven Elongation Monitor for Soft Devices Using a Deformation-Activated Piezoconductive Switch

*Yuji Isano, Munkhzaya Purevdorj, Nyamjargal Ochirkhuyag, Tamami Takano, Shoki Kato, and Hiroki Ota**

Stretchable devices have advanced in recent years, but challenges remain in managing deformations beyond design limits. Continuous power consumption for deformation monitoring hinders practical use. This underscores the need for a system capable of detecting loads beyond the allowable deformation of stretchable devices while minimizing energy consumption. Here, we developed a strain-induced switching circuit based on a positive piezoconductive composite. This composite transitioned from a resistance value exceeding 10 MΩ to a conductive state under strain, exhibiting a switching ratio of 10^5, enabling passive detection of excessive deformation, while it is decreased to 10^2 after 100 cycles of repeated use. The composite—made from silicone, ionic liquid, and nickel particles—offers tunable switching behavior by adjusting the nickel-to-polymer ratio and cross-sectional geometry. By combining it with a stretchable, non-contact power transfer system using printed liquid metal coils, we realized a low-energy, event-driven strain monitor embedded in stretchable devices. The liquid metal coils maintained stable power transmission even under 30% extension. We demonstrated applications in deformation detection of a plastic plate and strain-triggered infrared communication. This achievement is expected not only to significantly enhance the safety and reliability of stretchable devices but also to contribute to the development of energy-efficient, self-protective devices.

1. Introduction

In recent years, polymer-based electronic devices with high flexibility and deformability have attracted considerable attention. Due to their lightweight nature, softness, and strong biocompatibility, these devices have been applied to a wide range of biomechanical interfaces, including electronic skin,[1,2] wearable sensors,[3,4] and soft robots.[5–7] Research in this field is progressing beyond proof-of-concept demonstrations toward practical applications, as evidenced by advances in medical technologies[8] and the development of mass-production techniques for industrialization.[9]

Despite these advancements, the fragility of deformable devices compared to their rigid counterparts[10,11] remains a significant challenge for widespread adoption. Stretchable devices often lack an exterior casing to preserve their high deformability, or their substrate and outer layers are mechanically fragile. As a result, even minor external forces can induce strain beyond the design limits, leading to device failure or functional degradation. Additionally, stretchable functional elements mounted on these devices generally have lower strain limits than the substrate itself, making them susceptible to irreversible damage even if the substrate remains intact. Therefore, to ensure the stable operation and practical implementation of flexible devices, it is crucial to incorporate a system that alerts users to excessive deformations or functional abnormalities.

One of the greatest challenges in integrating such a warning system into stretchable devices is the energy supply. Various deformable energy sources, such as supercapacitors,[12,13] highly deformable batteries,[14,15] and energy harvesters[16–18] have been developed for stretchable systems. However, their energy densities remain lower than those of conventional solid-state batteries, making it difficult to sustain both the device's primary functions and additional strain-monitoring features over extended periods. Consequently, minimizing the system's energy consumption is essential.

From a device protection standpoint, an ideal strain measurement system should remain in an ultra-low-power standby mode under normal conditions, activating only when the

Y. Isano, M. Purevdorj, S. Kato
Department of Mechanical Engineering
Yokohama National University
79-5, Tokiwadai, Hodogaya-Ku, Yokohama, Kanagawa 240–8501, Japan
N. Ochirkhuyag, H. Ota
Institute for Multidisciplinary Sciences
Yokohama National University
79-5, Tokiwadai, Hodogaya-ku, Yokohama, Kanagawa 240–8501, Japan
E-mail: ota-hiroki-xm@ynu.ac.jp
T. Takano, H. Ota
Graduate School of System Integration
Yokohama National University
79-5, Tokiwadai, Hodogaya-Ku, Yokohama, Kanagawa 240–8501, Japan

The ORCID identification number(s) for the author(s) of this article can be found under https://doi.org/10.1002/admt.202500937

DOI: 10.1002/admt.202500937

deformation exceeds a predefined threshold. This functionality can be achieved through event-driven systems, which operate devices solely in response to specific events.[19] By eliminating continuous data measurements and large-scale data processing, event-driven approaches significantly reduce power consumption.[20,21] Such systems have also been utilized in wearable posture-monitoring devices, leveraging their inherently low power requirements.[22]

Here, we propose an event-driven stretchable strain monitor that remains in an ultra-low-power state and activates only when the strain surpasses a specified threshold. To achieve this, we utilized a positive piezoconductive composite whose conductivity increases by up to 10^5-fold once the strain exceeds a critical value. This enables the circuit to switch on only when necessary, eliminating the need for continuous sensing. We then integrated this strain switch with a stretchable, contactless magnetic-coupling power supply using liquid metal coils, creating a fully stretchable system. This approach is expected to enhance both the long-term stability and energy efficiency of stretchable devices, marking an important step toward the broader adoption of flexible electronic systems.

2. Result and Discussion

2.1. Event-Driven Stretchable Strain Monitor

A highly stretchable event-driven strain monitor capable of automatically activating a device only when an applied strain exceeds a predefined threshold was proposed (**Figure 1a**). The stretchable strain monitor comprises three main components: an event-driven circuit, a positive piezoconductive switch, and a stretchable wireless power supply system. The event-driven circuit includes functional elements such as transistors, a microcontroller unit (MCU), and LEDs, all mounted on a flexible polyimide substrate. The substrate of the device was made of silicone rubber material, and an event-driven control circuit constructed on a flexible substrate was integrated into the device using a hard-soft composite structure. The entire device was designed to be stretchable, although the control circuit was not. The positive piezoconductive switch described below was controlled by loading the device with a configured amount of strain.

The positive piezoconductive switches were composed of silicone rubber (Ecoflex), an ionic liquid, and nickel powder. These switches exhibited a rapid transition from an insulating to a conductive state when subjected to strain. Unlike conventional strain sensors, this composite material demonstrated a unique property—its conductivity increased sharply with elongational strain. Its high elasticity and steep conductivity change characteristics made it more suitable for switch-like applications rather than continuous sensing.

In its relaxed state, the composite maintained the circuit in a near-insulating state, allowing current to flow only when the applied strain exceeded a predefined threshold. As a result, the system's power consumption was significantly reduced in the absence of strain loading. Strain-induced switching was achieved using a voltage-divider circuit that combined the composite with a fixed resistor.

A stretchable wireless power transfer system was fabricated using a liquid metal coil and a charging IC, enabling contactless power transfer even under 30% elongation. Compared to existing microchannel-based fabrication methods,[23–25] the liquid metal coil was produced using a simpler mask-based printing process, which facilitated easier integration with external components such as flexible circuits and batteries. Incorporating wireless power transfer into event-driven devices enabled charging of embedded devices within structures or polymer materials, contributing to the development of low-power strain monitors for future elastic devices.

The switching mechanism of the event-driven stretchable device was implemented using a voltage-divider circuit with a fixed resistance, as described above (Figure 1b). The strain threshold at which the circuit was activated could be adjusted by varying the fixed resistance in the voltage divider. The output of the voltage divider circuit was connected to the MCU sleep-release trigger pin via a transistor (Figure 1b(i)). In the relaxed state, the MCU remained in sleep mode, consuming minimal power (Figure 1b(ii)). When the applied strain exceeded the threshold, the switch entered a conductive state, activating the FET and applying voltage to the trigger pin, thereby powering the circuit (Figure 1b(iii)).

This event-driven switching system eliminated the need for continuous monitoring of sensor resistance, enabling the circuit to activate only in response to strain events. As a result, the MCU's power consumption was reduced to less than 1/3000 of the power required for constant monitoring, significantly improving energy efficiency for long-term strain monitoring.

2.2. Characteristics of Positive Piezoconductive Switches

Positive piezoconductive switches, which exhibit a rapid increase in conductivity upon extensional strain, are the core components of event-driven strain monitors. The characteristics of this composite material, essential for its integration into an event-driven device, were investigated.

The composite material was fabricated using a simple mixing and molding process (**Figure 2a**). A mixture of Ecoflex 00–30, a type of silicone rubber, and a high concentration of nickel powder resulted in unique strain-dependent conductivity properties. The inclusion of ionic liquids caused the Ecoflex to swell, enabling a high maximum breaking strain despite the presence of a large amount of solid particles in the mixture (Figure S1, Supporting Information). Ecoflex, nickel powder, and the ionic liquid were placed in a vial i), mixed with a planetary mixer ii), and cured by molding iii, iv) to produce composites(Figure 2b).

The unique conductivity change property of this composite material was caused by a decrease in cross-sectional area under strain, as reported in a previous study[22] (Figure 2c). In the relaxed state, the silicone rubber matrix prevented sufficient contact between nickel particles, rendering the composite insulating. Upon elongation, the cross-sectional area decreased, leading to particle aggregation. This aggregation established conductive pathways, making the composite conductive. Given this principle, both the nickel particle ratio and the cross-sectional shape are crucial factors influencing the composite's electrical properties when applied in a device.

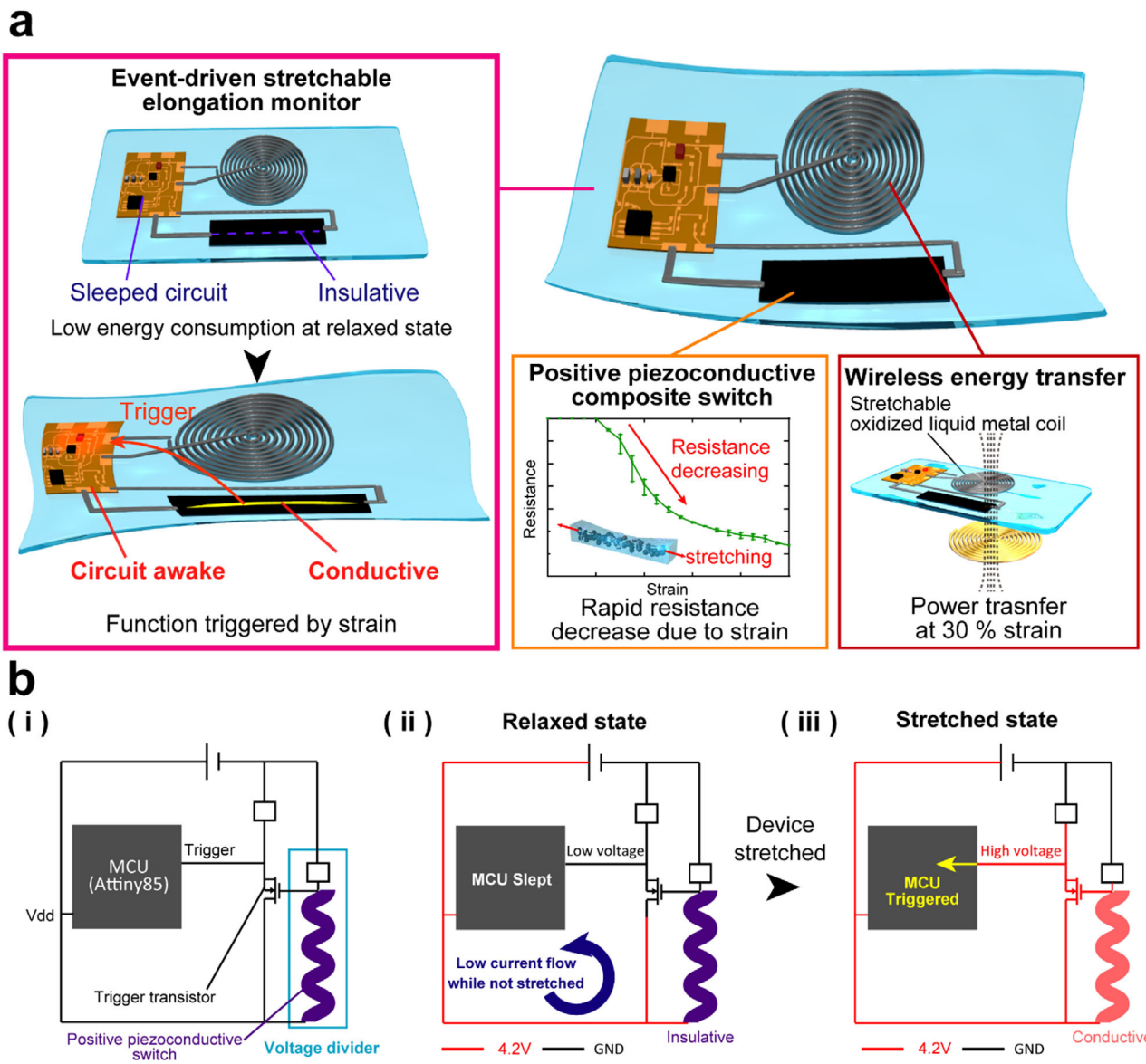

Figure 1. Overview of the event-driven stretchable elongation monitor. a) System description: A flexible circuit was mounted on a soft silicone substrate. During normal operation, the circuit remained in a low-power sleep state and was activated only when the positive piezoconductive switch transitioned to a conductive state upon extension. The system was powered by a flexible lithium-ion battery, which received energy through a deformable wireless power supply utilizing a liquid metal coil. b) Schematic of the event-driven switching circuit. i) Overall view of the circuit: In its relaxed state, the microcontroller unit (MCU) of the control circuit remained in sleep mode, while the strain switch was in an insulating state, effectively interrupting the circuit. ii) When the applied strain exceeded the threshold of the positive piezoconductive switch, a voltage was supplied to the MCU's activation trigger, switching the circuit on. iii) This activation enabled the system's functionality, responding only to strain events above the predefined threshold.

To evaluate the switching characteristics, the strain-resistance relationships for different polymer-to-nickel mass ratios were examined (Figure 2d). A rapid increase in conductivity with tensile strain was observed when the nickel mass exceeded twice that of the polymer, confirming positive piezoconductivity. However, repeated straining led to a gradual decline in conductivity, and eventually, conductivity was no longer achieved (Figure S2, Supporting Information). Additionally, when the nickel mass exceeded 3.5 times that of the polymer, polymer curing was inhibited, preventing composite formation.

Conversely, when the nickel mass was less than twice the polymer mass, the conductivity increase with strain was moderate, and positive piezoconductivity was not observed when the polymer-to-nickel mass ratio was 1:1. Notably, composites with a 1:1.5 polymer-to-nickel ratio exhibited significant variability in strain-conductivity characteristics, showing a large error range. This behavior likely resulted from sample-to-sample variability, particularly in the threshold at which resistance began to drop. These results suggest that positive piezoconductivity is influenced by a probabilistic percolation phenomenon among nickel particles in the composite.[26] Because conduction through

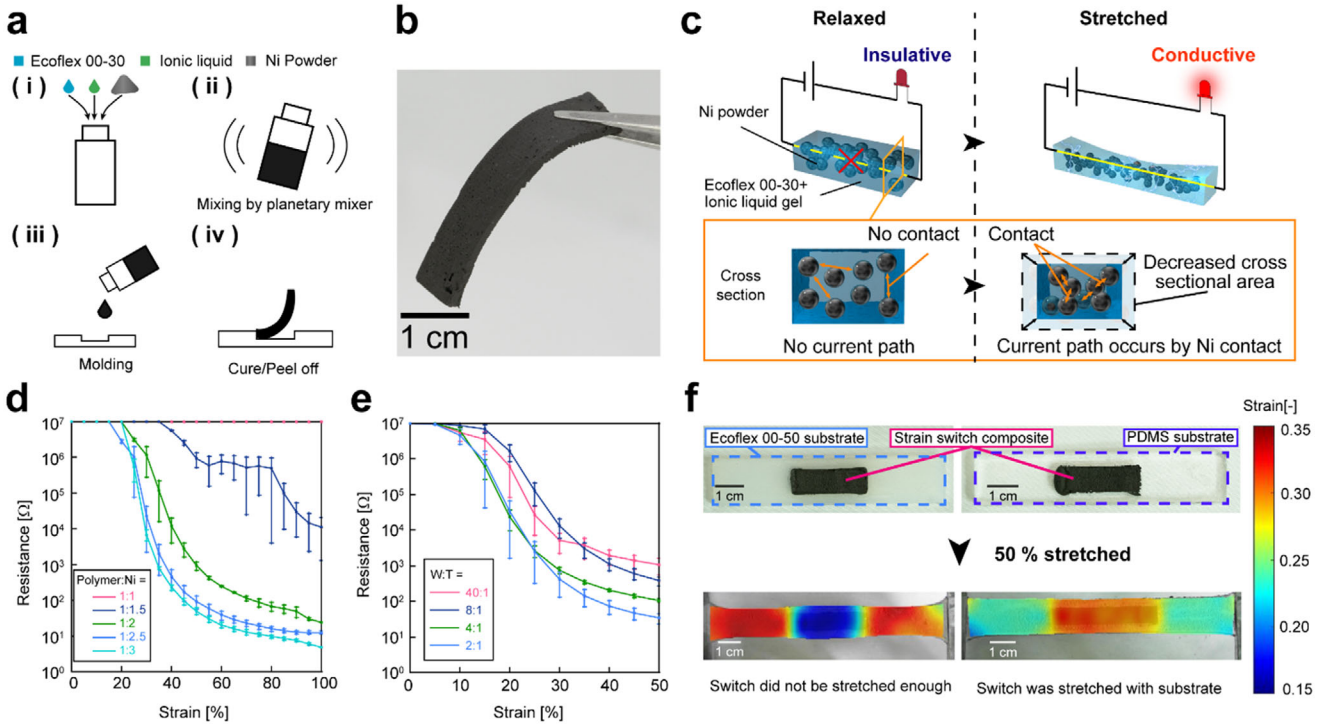

Figure 2. Positive piezoconductive switch composite. a) Fabrication process of positive piezoconductive composites. The composite was created by mixing Ecoflex 00–30, nickel powder, and an ionic liquid, followed by molding and curing. b) Fabricated positive piezoconductive composite. The final composite exhibited strain-dependent conductivity properties suitable for event-driven applications. c) Principle of positive piezoconductivity. Tensile strain caused a reduction in cross-sectional area, decreasing the distance between nickel particles and forming conductive pathways. d) Strain–resistance relationship as a function of polymer-to-nickel mass ratio. Positive piezoconductivity was observed at polymer-to-nickel mass ratios of 1:2 or higher. Error bars indicate the standard error for three samples. e) Strain–resistance relationships for samples with different cross-sectional geometries. Samples with thicknesses of 0.2, 1, 2, and 4 mm (all 8 mm in width) were analyzed. A higher cross-sectional aspect ratio corresponded to a higher strain threshold for the onset of resistance reduction. Error bars represent the standard error for five samples. f) Deformation characteristics of positive piezoconductive switches combined with substrates of varying stiffness. When subjected to 50% strain, switches with an Ecoflex substrate exhibited < 20% deformation, while those with a PDMS substrate deformed by ≈30%.

percolation exhibits a sharp transition around a critical conductor concentration, reducing the number of conductive particles shifts the variability distribution toward this threshold, making small differences in sample composition significantly impact conductivity.

Table S1 (Supporting Information) summarizes the sensitivity of each composite. The sensitivity calculation for the positive piezoelectric composite was divided into four regions: the insensitive region immediately after deformation begins, the high-sensitivity region near the threshold, the low-sensitivity region in the saturated state, and the intermediate sensitivity region between the high- and low-sensitivity regions. Consequently, the results show that increasing the nickel content enhances sensitivity in the high-sensitivity region while decreasing sensitivity in the intermediate and low-sensitivity regions. Considering the need for a steep resistance change when operating as a switch, these findings suggest that higher nickel content improves the switching characteristics. In this study, a polymer-to-nickel ratio of 1:2 was selected to provide an appropriate resistance change range while allowing effective threshold adjustments via the voltage divider circuit.

The effect of the cross-sectional aspect ratio on strain-conductivity characteristics was also investigated. The cross-sectional width was fixed at 8 mm, while thicknesses of 0.2, 1, 2, and 4 mm were tested (Figure 2e). Results showed that the strain threshold for resistivity reduction decreased as thickness increased. The lowest error range in resistance change was observed at a thickness of 2 mm, while the error increased for both thinner and thicker samples. The decrease in strain threshold with reduced thickness is likely due to a lower probability of conductive path formation in the thickness direction. Meanwhile, the increase in error range was attributed to different causes depending on thickness: for thinner samples, variability was linked to the percolation threshold, similar to low-nickel-ratio samples. For thicker samples, the difficulty of uniformly filling the mold with the uncured composite likely caused macroscopic inconsistencies among samples. Given the importance of stable electrical properties in device applications, a 2 mm thickness was chosen for the positive piezoconductive switches in this study.

Finally, the response speed of the positive piezoconductive composite was measured (Figure S3, Supporting Information). Within 100 ms after the strain reached the threshold, the resistance value decreased by over 97%. Furthermore, when the strain reached 50%, the change in resistance had almost converged. This response speed is sufficient for using the positive piezoconductive composite as a strain switch. Additionally, the strain

detection characteristics of positive piezoconductive composites under ambient conditions were examined (Figure S4, Supporting Information). The results showed that temperature changes caused a difference of ≈5% in the strain state at the same resistance value, while no significant effect was observed for humidity changes. For practical device applications, it is necessary to adjust the threshold on the circuit side to account for potential temperature, humidity changes, and the acceptable strain range.

Elasticity matching with the device substrate is crucial for investigating the switching behavior of positive piezoconductive switches in stretchable-device applications. We examined the stretchability of the switches using Ecoflex 00–50 and PDMS as device substrates, which have higher and lower Young's moduli than the switches, respectively (Figure 2f). The results showed that switches with Ecoflex substrates expanded by less than 20% when subjected to 50% strain, whereas those with PDMS substrates expanded by ≈30%. The switches with Ecoflex substrates remained insulating under 50% strain, while those with PDMS substrates were in a transition state between insulating and conducting, with a resistance of ≈100 kΩ. This suggests that the strain threshold for event-driven switching can be manipulated not only by controlling the nickel content of the switch but also by changing the substrate material.

The Young's moduli of Ecoflex 00–50, PDMS, and the positive piezoconductive switch used in this study were 0.1 MPa[27], 2.6 MPa,[28] and 0.3 MPa, respectively. Considering that the cross-sectional area of the composite in the center part of the sample is 25% of the entire sample, the combined law of Young's modulus for dissimilar joint surfaces yielded values of 2.025 MPa for the PDMS-composite part and 0.15 MPa for the Ecoflex-composite part. Simple strain distribution modeling, without considering junction boundary effects, showed that the strain in the switch section was ≈25% of the total substrate strain when an Ecoflex substrate was used. In contrast, when a PDMS substrate was used, the strain at the switch accounted for 39% of the total substrate strain. Although the actual device did not perfectly match the theoretical model due to strain distribution gradients at the junction boundary, the deformation state of the switch was influenced by the surrounding materials of different stiffnesses. This demonstrates that the strain applied to the switch can be controlled by modifying the substrate material.

Several composite materials with positive piezoconductivity have been reported,[29–32] but they all face a trade-off between deformation capability and resistance change rate. The composite used in this study achieves high elongation resistance of more than 100% while maintaining an ON/OFF resistance ratio exceeding 10^5, as previously reported.[22] This property is essential for event-driven strain monitoring in highly deformable devices. In this study, we demonstrated the controllability of the electrical properties of positive piezoconductive composites using a material-property-independent approach by analyzing shape-dependent electrical properties and deformation characteristics in relation to substrate stiffness.

However, poor cyclic stability (Figure S2) posed a major challenge for device fabrication: the resistance ratio under the same strain before and after testing decreased from $1/10^5$ to $1/10^2$ after 100 cycles of 50% strain. This degradation was primarily attributed to fatigue softening of the silicone rubber.[33,34] This result is supported by the observed variations in stress during repeated stretching of the positive piezoconductive composite (Figure S5, Supporting Information). The data suggest that the reduction in internal stress due to repeated elongation reduces the force applied to the nickel particles embedded in the composite. This deteriorates the repeated characteristics by dampening the movement of the nickel particles.

Addressing this issue requires minimizing fatigue softening of the silicone rubber matrix, and fundamental improvements are unlikely without advances in materials engineering. Efforts to enhance cyclic stability by modifying conductive fillers have been explored, with liquid metal additives yielding positive piezoconductive composites with improved repeatability.[30] However, such studies have been limited to cyclic strains of ≈10%. The effects on composites subjected to strains exceeding 50%, as in this study, remain unexplored.

To enhance repeatability through matrix optimization, it is plausible to use materials that undergo structural changes in their chain structure when heated, such as shape memory polymers and poly(N-isopropylacrylamide) (PNIPAM) hydrogels, or thermoplastic polymers, as the matrix. These materials may enable recovery of the electrical properties of positive piezoconductive composites by facilitating polymer chain reorientation through heating. Nevertheless, the application of such composite materials should be considered not only to enhance switch performance but also from the perspective of circuit design and practical use.

2.3. Wireless Power Transfer System Using Liquid Metal Coils

Possible applications for event-driven strain monitors include structural deformation monitoring systems that can be embedded in soft structures to detect abnormal strains. For this purpose, a deformable power supply system without external wiring is necessary. In this study, a wireless power supply system based on magnetic field coupling using liquid metal coils was developed and applied as an energy source for an event-driven strain monitor. The characteristics and fabrication of the liquid metal coil, which forms the core of the wireless power supply system, were discussed.

The liquid metal coils used for wireless power transfer were fabricated using a mask-printing process (**Figure 3a**). While injection into fluidic channels[23–25] and spray coating[35] have previously been used to fabricate liquid metal coils, the mask-printing process employed in this study facilitated integration with other device elements, such as flexible circuit boards and positive piezoconductive switches.

In mask printing, simply placing a mask on a polymer substrate can cause the mask to shift during printing, leading to deformation of the coil shape. To prevent this, the mask was stabilized by molding the substrate onto a polyimide mask with premade incisions to maintain coil integrity (Figure 3a). An Ecoflex layer was prepared at the bottom of the mold to secure the mask in place i). A mask with a coil pattern cut into it was fixed onto the Ecoflex layer ii), and PDMS was poured from the top to fabricate the substrate iii). Once cured, the PDMS and mask were peeled off from the mold and inverted iv), and the incised area was removed to complete the mask v). Liquid metal paste ink was then spread over the mask vi), after which the mask was peeled off to

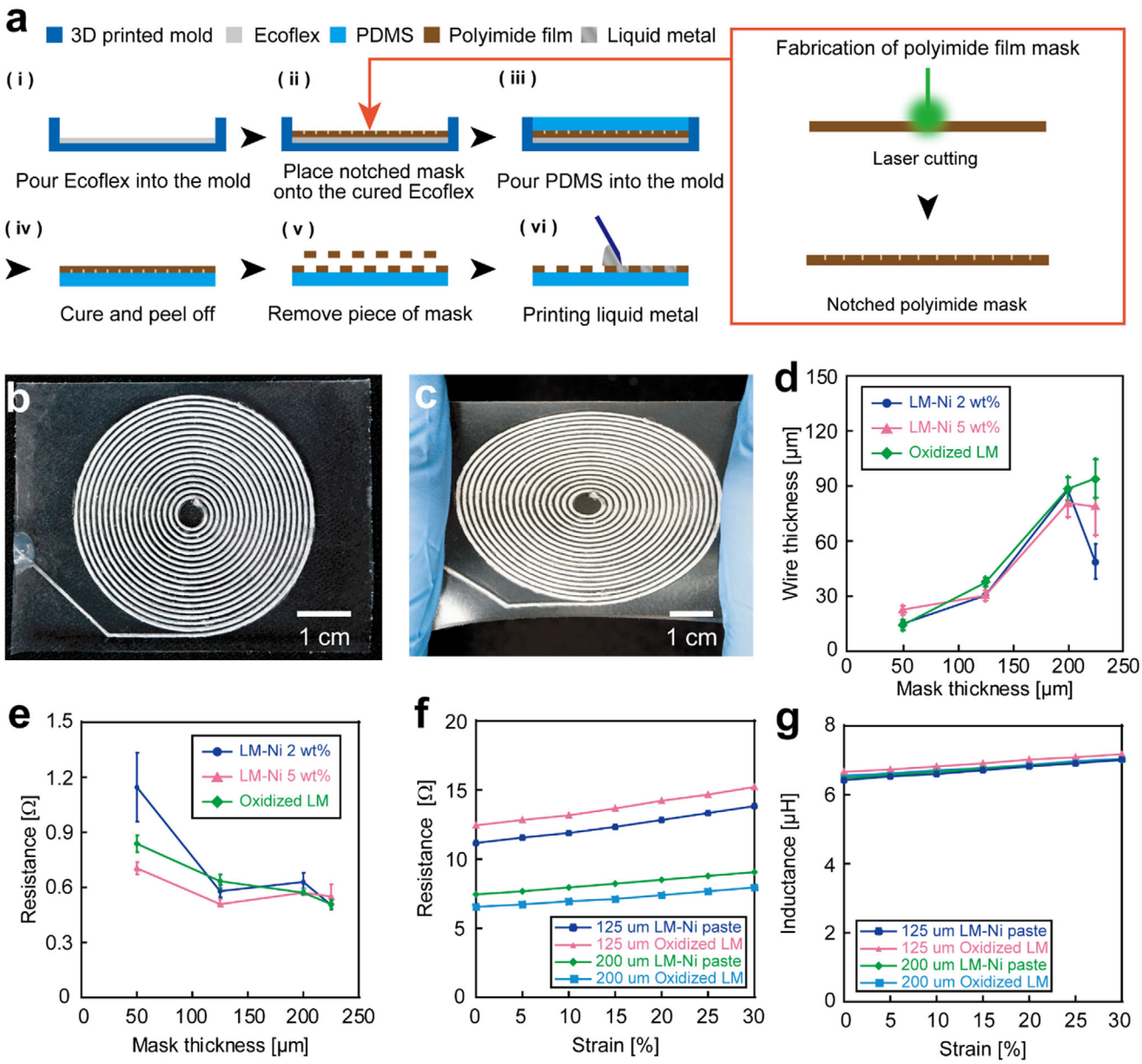

Figure 3. Liquid metal stretchable coil. a) Fabrication process of a liquid metal coil. b,c) Fabricated liquid metal coils in (b) relaxed and (c) at 30% strain states. d, e) Wiring thickness (d) and wiring resistance (e) compared with mask thickness. The wiring coil was fabricated with a width of 0.5 mm and a length of 40 mm. The wiring thickness increased uniformly up to a mask thickness of 200 μm, but became unstable at 225 μm. Resistance decreased with increasing mask thickness but saturated at 125 μm. The error bars indicate standard errors from (d) five different measurement points on one sample and (e) four different samples. f,g) Variation of resistance (f) and inductance (g) with coil strain. The resistance of the coil varied with mask thickness regardless of ink type and increased with elongation. Inductance increased slightly with elongation.

finalize the coil. The fabricated coils are shown in Figure 3b,c. The coil was designed with 19 turns, a wire width of 0.5 mm, and a wire-to-wire spacing of 0.5 mm. It maintained functionality under 30% elongation without liquid metal leakage or wire contact.

To achieve high-performance wireless power transfer, minimizing coil resistance loss and increasing inductance are crucial. Although inductance could be improved by increasing the number of turns and wiring density, fabrication constraints limited the extent of enhancement. On the other hand, reducing coil resistance loss was more feasible by increasing wiring thickness and optimizing the liquid metal material. In this study, several liquid metal inks and mask thicknesses were evaluated based on their printing and electrical characteristics to optimize wiring thickness and material selection. To examine the impact of fillers on conductivity and the effect of magnetic materials on inductance, pure liquid metal, liquid metal-nickel mixtures with 2% and 5% nickel by mass, and oxidized liquid metal were tested.

A simple linear pattern was used to measure wiring thickness for different mask thicknesses (Figure 3d). Up to a mask thickness of 200 μm, the wiring thickness of all pastes increased

proportionally with mask thickness. However, at 225 μm, the wiring thickness decreased for the nickel-containing inks. Although the average thickness of oxidized liquid metal increased, the variation was not significant, given the larger error range. In the case of printing with pure liquid metal (Figure S6a, Supporting Information), unstable wiring thickness was observed, even with a thin mask, compared to paste ink. Patterns printed with pure liquid metal had difficulty maintaining their shape due to surface tension effects.

Next, the change in wiring resistance at different mask thicknesses was examined using a linear pattern (Figure 3e). In all cases, resistance decreased as mask thickness increased but saturated at ≈0.6 Ω. This suggests that the contact resistance ratio increased due to the short wiring pattern, making it difficult to accurately observe the change in resistance with film thickness. In the case of pure liquid metal printing (Figure S6b, Supporting Information), wiring resistance remained lower than that of other materials across all mask thicknesses. Based on these findings, 200 and 125 μm masks were selected for the coil shape study as they provided stable wiring thickness with all paste ink materials except pure liquid metal. Additionally, 2% Ni-LM paste and oxidized liquid metal, which exhibited similar wiring thicknesses with the 200 μm mask, were chosen to investigate the effect of magnetic material content on inductance.

Coils were fabricated using four different combinations of mask thickness and liquid metal ink, and their resistance and inductance were evaluated under up to 30% elongation. As shown in Figure 3f, coil resistance decreased with increasing mask thickness, while differences in resistance due to liquid metal type were smaller than those caused by film thickness. A notable difference in resistance emerged when the coil was formed into a long wiring length. The maximum resistance change during coil elongation was ≈1.2 times, demonstrating the stability of the liquid metal coil's electrical characteristics under mechanical deformation.

Figure 3g shows the change in inductance when the coils are subjected to extensional strain. The inductance values of all coils were almost the same, regardless of the presence or absence of the magnetic material and the thickness of the coil. The inductance increased slightly as the coils were elongated (Figure S7, Supporting Information). The inductance of the flat coil was approximated using the following equation,[36]

$$L = r^2 \times n^2 / (8 \times r + 11 \times w) \quad (1)$$

where r is the radius of the center of the windings, w is the width of the windings, and n is the number of turns. Applying this formula to the coil in this study, the estimated inductance at relaxation was 6.71 μH, which was almost the same as the experimental value. From this result, it can be concluded that the inductance of a liquid-metal coil is determined by its shape. In other words, the material could be selected based on its ease of fabrication because the material of the liquid metal ink did not affect the inductance. The increase in inductance with coil elongation was assumed to be due to an increase in the coil center radius r.

Based on the above considerations, 200 μm mask film thickness was selected as the maximum film thickness that can be processed stably, and liquid metal oxide paste was selected as the ink material due to its ease of fabrication. The optimized coil was subjected to 120 cycles of 30% repetitive tensile testing (Figures S8 and S9, Supporting Information). As a result, a 0.1% decrease in inductance and a 0.3% increase in resistance were observed before and after the repetition test. Liquid metal coils exhibit high deformability, which allows them to be embedded in stretchable devices that repeatedly deform.

2.4. Integrated Event-Driven Strain Monitor

An event-driven strain monitor was fabricated by integrating a positive piezoconductive strain switch, liquid metal coil, and control circuit (**Figure 4**a,b; Figures S10 and S11, Supporting Information). A flexible circuit board and a molded positive piezoconductive switch were bonded to a PDMS substrate, on which a liquid metal coil was printed. The control circuit for event-driven operation, a charging circuit, and a flexible lithium-ion battery were mounted on the flexible circuit board. The coils and strain switches were connected to the circuit via printed wiring using a liquid metal paste, with rigid silicone rubber applied at contact points to prevent breakage during extension.

The event-driven strain monitor comprised three functional components: charging, strain detection, and strain-triggered response (Figure S12, Supporting Information). The charging component received power via magnetic coupling between the liquid metal coil and an external coil, directing it to a flexible lithium-ion battery through a rectifier IC. The strain detection component used a voltage divider circuit to monitor deformation, consuming minimal power due to the high resistance of the strain switches. The functional component included an MCU and LEDs, with the MCU kept in deep sleep to minimize power consumption. Upon activation by a voltage input from the strain detection circuit, the MCU triggered the LEDs to operate according to a programmed pattern, either for external communication or indicator lighting.

The charging performance of the contactless power transfer system using liquid metal coils was evaluated (Figure 4c,d; Figure S13, Supporting Information). The charging current was regulated at 10 mA (≈0.1 C) by a charging IC, with measurements recorded every 0.1 s and their 30-s moving averages displayed. The average charging current was 7.5 mA in the relaxed state and 5 mA under 30% extension (Figure 4c), leading to a 25% increase in charging time during stretching (Figure 4d).

The reduction in charging efficiency under strain was attributed to an increase in coil resistance and a decline in magnetic coupling. At 30% strain, coil resistance increased by 17%, and inductance by 7% (Figure 3f,g). At a resonance frequency of 100 kHz, the Q-value decreased by ≈10% due to these resistance and inductance changes. Additionally, coil deformation during extension caused a shape mismatch with the power transmission coil, increasing leakage flux and reducing the coupling coefficient. Despite these effects, the liquid metal coil enabled continuous contactless power transfer under extensional strain.

To demonstrate the functionality of the device, deformation monitoring was performed using a highly deformable plastic plate (Figure 4e; Movie S1, Supplementary Movie1). The device was affixed to the plastic plate, which was then subjected to bending deformation (Figure 4e(i)). When the strain switch deformation remained below the threshold, the event-driven circuit remained dormant, and the functional elements—the LEDs—did

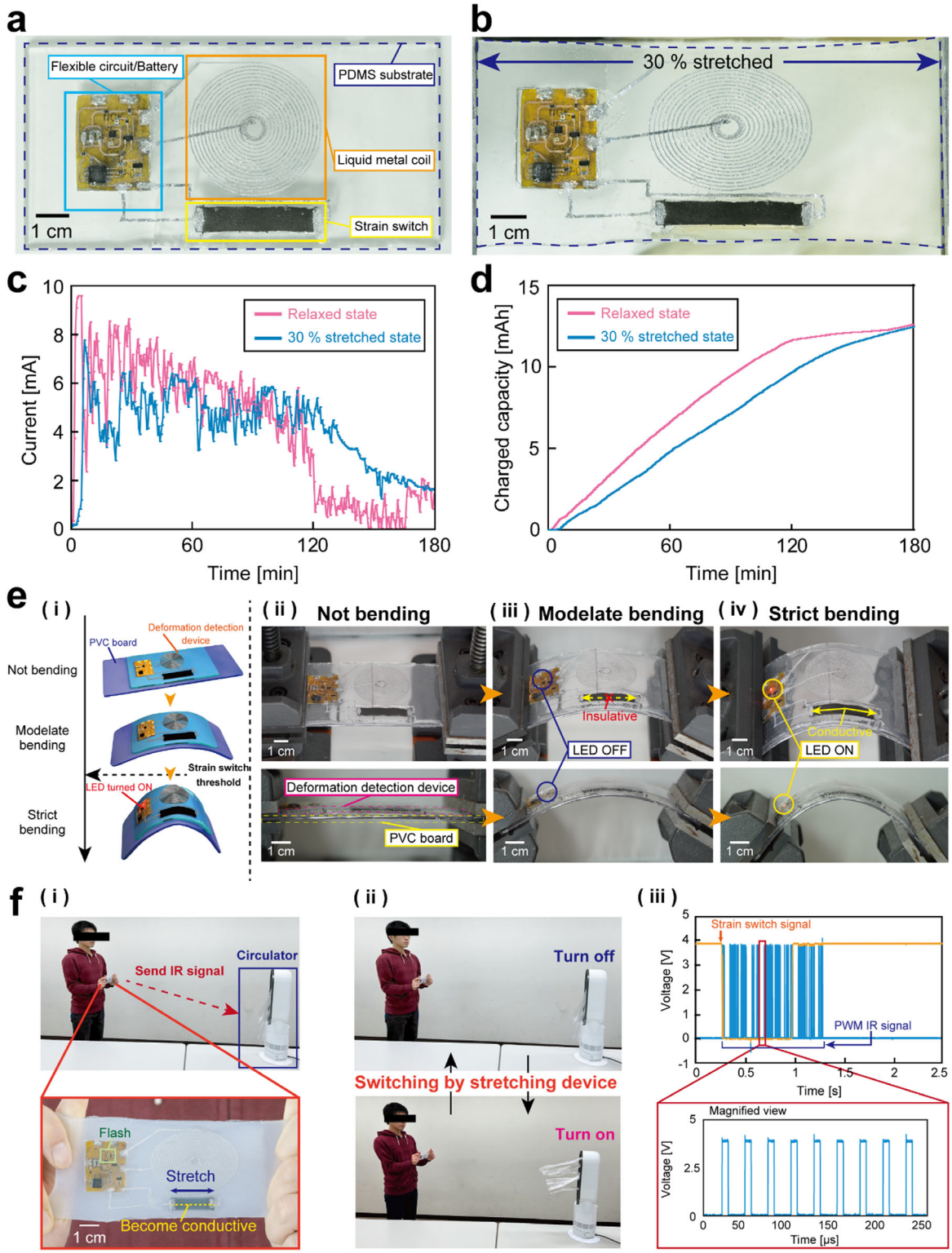

Figure 4. Integrated event-driven elongation monitor. a,b) Entire image of the elongation monitor. (a) relaxed, (b) 30% stretched condition. c,d) Wireless charging performance of the device; charging current (c), total charged capacity (d) through time. Charging efficiency at 30% strain was 25% worse than at relaxation. e) Structural deformation monitoring demonstration. i) Demonstration overview. When the device was not deformed sufficiently, the positive piezoconductive composite was insulating ii, iii), whereas large deformation changed it to conductive and activated the functional circuit iv). f) strain-induced infrared communication. i) Demonstration overview. The event-driven circuitry in the device, which controlled the circulator, was triggered by causing the IR LEDs to blink in a programmed pattern ii). iii), MCU activation trigger and IRLED voltage when the event-driven strain monitor was activated.

not light up (Figure 4e(ii),(iii)). However, when the bending deformation exceeded the threshold, the MCU was activated, causing the LEDs to illuminate (Figure 4e(iv)). The device remained intact and fully operational even under repeated bending, continuing to function until the plastic plate fractured.

It is theoretically feasible to fabricate a device capable of detecting different curvature thresholds. These thresholds can be adjusted by varying parameters such as the material mixing ratio of the strain switch, the resistance value of the voltage divider resistor, and the length of the strain switch. However, in practical applications, factors such as the wide error range of the strain switch and individual differences in circuit elements may hinder accurate threshold setting. To prevent these influences, the threshold of the voltage divider resistor should be set to a value that is sufficient after the resistance value of the strain switch has decreased adequately. For curvature detection, adjusting the length of the strain switch to control the strain experienced at the same curvature is an effective approach.

The event-driven strain monitor can be adapted for advanced functions by modifying its on-board functional components. As a demonstration, the device was used to activate a remote-controllable electrical system via infrared communication (Figure 4f(i); Movie S2, Supplementary Movie2). The device was equipped with an infrared LED that controlled a circulator by blinking in a pattern pre-programmed into the MCU when strain exceeded the threshold (Figure 4f(ii)). The voltage responses at the IR LED and MCU trigger pins under strain conditions are shown in Figure 4f(iii). When the strain on the voltage divider circuit exceeded a critical level, the MCU trigger turned on, activating the infrared LED to blink in a predefined communication pattern.

In this study, deformation was used as an event-driven trigger to control other devices. Previous research has reported strain-induced logic gates utilizing vapor-deposited metal and ultrathin polydimethylsiloxane (PDMS) films as highly stretchable ON-switch[37] devices. Similarly, twisted conductive fibers have been employed to create strain-responsive ON-switch devices.[38] These approaches have demonstrated high repeatability and ON/OFF resistance ratios of 10^9 and 10^8, respectively, making them promising for event-driven circuits. However, fabrication challenges exist for both methods: the vapor deposition approach requires a long-duration high-vacuum treatment, while the fiber-based method necessitates complex chemical treatment and precise fiber alignment, making it difficult to integrate with conventional stretchable device fabrication. Another example of an integrated system utilizing mechanical deformation, energy sources, and functional elements is a stretchable lithium-ion battery combined with pressure switches and electronic circuits.[39] While this approach successfully integrates extendable batteries, sensors, and circuits, it does not incorporate an external charging system.

In contrast, our study developed a liquid metal wiring and wireless power transfer coil via a simple printing process and integrated them with a strain switch that can be fabricated through polymer casting and curing. This enables a fully integrated power supply and switching system that can be configured on various stretchable substrates using a straightforward fabrication method. This feature presents a significant advantage for the future development of strain monitoring systems in diverse stretchable electronic applications.

Positive piezoconductive composites can be integrated into more complex systems by incorporating the composite directly into the gate of a stretchable transistor to form an active matrix or by creating a simple passive matrix. However, applications such as node-by-node pressure measurement using existing implementation methods have limited significance, as they do not utilize the unique switching behavior of positive piezoelectric conductive composites in response to elongational strain. To apply this specificity in array devices, it will be necessary to construct devices that are not bound by existing node-by-node measurements, such as covering the entire array device with positive piezoconductive composites and estimating local elongation of the device by measuring the conductivity between the nodes.

3. Conclusion

In this study, we developed an event-driven, stretchable strain monitor by integrating a positive piezoconductive strain switch with a stretchable wireless power transfer system. Systematic investigations of the nickel content and geometric structure clarified the steep strain–conductivity behavior of the switch and demonstrated that the overall switching threshold could be flexibly tuned through voltage divider circuit design and careful selection of peripheral materials. Additionally, a stretchable liquid metal coil enabled continuous wireless power transmission even under 30% elongation, verifying the robustness of the proposed power delivery architecture.

Functional demonstrations showed that the integrated device can simultaneously perform event-triggered structural deformation monitoring and infrared communication, highlighting its potential for low-power fault detection in emerging soft electronics. Notably, its ability to regulate current output based on applied strain suggests the feasibility of a software-independent autonomous control mechanism, particularly in combination with soft robotic systems such as balloon actuators. This capability opens new avenues for achieving intrinsically adaptive functionalities in wearable and soft robotic applications.

However, the limited durability of positive piezoconductive strain switches remains a significant challenge. Real-time microscopic observation of particle motion within the switching layer could provide crucial insights into the mechanisms behind positive piezoconductivity and the root causes of degradation under repeated loading. Such findings could be instrumental in enhancing device performance and reliability.

Conversely, positive piezoelectric conductive composites may be valuable for developing devices that utilize nonlinear resistance changes and characteristic degradation during repeated use, such as in neuromorphic sensing[40]. By linking the degradation of sensitivity characteristics to the adaptation mechanism of biological sensory nerves and utilizing these effects as memory functions, it is possible to develop new low-energy consumption sensing systems that utilize the characteristics of these composites. By leveraging these insights, future research may focus on refining both material systems and device architectures, ultimately paving the way for highly reliable, low-power, and continuously functional soft electronic systems across diverse application fields.

4. Experimental Section

Fabrication of Positive Piezoconductive Switch: Positive piezoresistive switches were fabricated by mixing silicone rubber (Ecoflex 00–30, Smooth-On), an ionic liquid (N-Methyl-N-propylpyrrolidinium bis(trifluoromethanesulfonyl)imide, Kanto Chemical), and nickel powder (<20 µm, Sigma-Aldrich) following a previously established method (Figure 2b) [1]. First, Ecoflex 00–30 components A and B were combined in a vial at a 1:1 mass ratio. The ionic liquid and nickel powder were then added at mass ratios of 0.1 and 1 to 3, respectively, relative to the total polymer content (Figure 2b(i)). The mixture was homogenized using a spin-orbit mixer (Thinky, ARE-310) at 2000 rpm for 4 min (Figure 2b(ii)). The resulting paste-like uncured composite was then poured into a 3D-printed mold and cured in an oven at 70 °C for 1 h (Figure 2b(iii)). Finally, the cured positive piezoresistive switch was carefully removed from the mold.

Evaluation of Positive Piezoconductive Switch: The deformation state of positive piezoresistive switches was evaluated on different substrate materials (Figure 2c), including PDMS (SYLGARD 184, Dow Corning, base: curing agent = 10:1) and Ecoflex 00–50 (Smooth-On, agent A: B = 1:1). The substrates were fabricated via molding, with an indentation formed to accommodate the switch. The paste-like uncured composite was then deposited into the cavity and cured in an oven at 70 °C for 1 h, resulting in a substrate-integrated switch.

Strain distribution analysis of the substrate was performed by digital image correlation (DIC). A random pattern was formed on the sample using black spray. The patterned sample was continuously subjected to an extensional strain at a rate of 1 mm/s. The process was captured using a video camera and converted into intermittent images every second. Finally, autocorrelation analysis was performed using DIC software (Ncorr, Matlab).

The electrical resistance change in the positive piezoresistive switches was measured using a tester (DT4261, HIOKI). Characterization of the polymer-nickel mass ratio (Figure 2d) was performed on an 8 mm wide, 40 mm long, and 2 mm thick sample. Characterization with varying thicknesses (Figure 2e) was performed on samples with a polymer-nickel mass ratio of 1:2, a width of 8 mm, and a length of 40 mm at thicknesses of 0.2, 1, 2, and 4 mm.

Response time of the positive piezoelectric conductive composites was measured by recording the current every 1 ms using a semiconductor parameter analyzer (B1500A, Keysight) while applying strain. Measurements of the positive piezoconductive composite properties in response to variations in the surrounding environment were conducted using an environmental chamber (SH-241, Espec).

Fabrication of Liquid Metal Ink: Liquid metal-nickel ink was prepared as follows: Ni powder (3–7 µm, Alfa Aesar Co.) at mass ratios of 2% and 5% was dispersed in Galinstan (materialsmith.com) and sonicated using an ultrasonic probe (SFX 550, BRANSON) at a duty cycle of 30%, with a total energy input of 6 kJ. The ink was then exposed to air overnight to accelerate oxidation.

Oxidized liquid metal ink was prepared by stirring Galinstan with a mechanical stirrer (Azone) at 750 rpm for 60 min in air.

Fabrication of Integrated Device: A flexible circuit board incorporating charging and control circuits was fabricated using a photolithography process. The LTC4124 (Analog Devices) was used as the charging IC, and the power received by the liquid metal coil was supplied to the battery. Functional components, including an MCU (Attiny85) and LEDs, were mounted on the circuit, along with fixed resistors and transistors forming the voltage divider circuit of the strain switch (Figure S7, Supporting Information).

The device substrate was fabricated using the same molding method as the liquid metal coil (Figure S11a, Supporting Information). After forming the coil on the substrate, a flexible circuit board and a positive piezoconductive strain switch were bonded (Figure S11b(i,ii), Supporting Information). The outer edges of the flexible substrate were reinforced with Dow 734 silicone rubber, which is harder than the substrate material. This reinforcement moderated the strain gradient during stretching, preventing rupture of the liquid metal wiring connections. Subsequently, part of the coil was covered with substrate material to join the coil's center to the flexible circuit (Figure S11b(iii), Supporting Information). The liquid metal coil and strain switch were then connected to the flexible circuit using oxidized liquid metal paste (Figure S11b(iv), Supporting Information). The contact points between the oxidized liquid metal paste and both the flexible circuit and strain switch were sealed using Dow 734 silicon rubber (Figure S11b(v), Supporting Information). Finally, the entire device was encapsulated in silicone rubber to complete fabrication (Figure S11b(vi), Supporting Information).

Evaluation of the Integrated Device: Charging performance was evaluated using a power transmission circuit with the LTC4125 (Analog Devices). The power transmission frequency was tuned to the resonant frequency using the LTC4125. Charging was performed with the device in direct contact with the power transmission coil, and the charging current on the device side was set to 10 mA. The battery anode current and anode-cathode voltage were recorded using a data logger (GL240, GLAPHTEC).

Structural deformation was assessed by bending and affixing the device to a PVC board. When the applied strain reached a predefined threshold, determined by the fixed resistance of the voltage divider circuit, a voltage signal was sent to the MCU, which activated the LED via the control program.

A remote control demonstration was conducted using a device equipped with an infrared LED and an MCU programmed with pulse-width modulation control software. When the strain exceeded the defined threshold, the infrared LED blinked in a predetermined pattern, enabling the device to transmit commands to an external system via infrared communication.

Supporting Information

Supporting Information is available from the Wiley Online Library or from the author.

Acknowledgements

This study was supported by the Japan Science and Technology Agency (JST) Advanced Integrated Intelligence Platform Project (No. JPMJCR22U2), Japan Society for the Promotion of Science (JSPS) KAKENHI Grant-in-Aid for Transformative Research Areas (No. 24H00890), and a Grant-in-Aid for Scientific Research A (No. 20H00213). The authors would like to thank Editage (www.editage.jp) for English language editing.

Conflict of Interest

The authors declare no conflict of interest.

Author Contributions

Y.I. performed conceptualization, investigation, data curation, formal analysis, software, visualization, and writing-original draft. M.P. performed the investigation, methodology, and formal analysis. N.O. performed the investigation, methodology, and formal analysis. T.T. performed methodology, software. S.K. performed conceptualization, investigation, data curation, and formal analysis. H.O. performed supervision, project administration, funding acquisition, conceptualization, writing review, and editing.

Data Availability Statement

The data that support the findings of this study are available from the corresponding author upon reasonable request.

Keywords

event-driven system, liquid metal, positive piezoconductive composite, stretchable device

Received: May 2, 2025
Revised: July 5, 2025
Published online:

[1] P. Makushko, J. Ge, G. S. Cañón Bermúdez, O. Volkov, Y. Zabila, S. Avdoshenko, R. Illing, L. Ionov, M. Kaltenbrunner, J. Fassbender, R. Xu, D. Makarov, *Nat. Commun.* **2025**, *16*, 1647.
[2] Y. Shang, C. Huang, Z. Li, X. Du, *Adv. Funct. Mater.* **2025**, *35*, 2412703.
[3] S. Liu, Y. Wu, L. Jiang, W. Xie, B. Davis, M. Wang, L. Zhang, Y. Liu, S. Xing, M. D. Dickey, W. H S Bai, *ACS Appl. Mater. Interfaces* **2024**, *16*, 46538.
[4] S. Lee, J. Kim, I. Yun, G. Y. Bae, D. Kim, S. Park, I. M. Yi, W. Moon, Y. Chung, K. Cho, *Nat. Commun.* **2019**, *10*, 1.
[5] S. J. Woodman, D. S. Shah, M. Landesberg, A. Agrawala, R. Kramer-Bottiglio, *Sci. Robot.* **2024**, *9*, 6844.
[6] S. Ma, P. Xue, C. Valenzuela, X. Zhang, Y. Chen, Y. Liu, L. Yang, X. Xu, L. Wang, *Adv. Funct. Mater.* **2024**, *34*, 2309899.
[7] D. Hu, F. Giorgio-Serchi, S. Zhang, Y. Yang, *Nat. Mach. Intell.* **2023**, *5*, 261.
[8] H. Xu, W. Zheng, Y. Zhang, D. Zhao, L. Wang, Y. Zhao, W. Wang, Y. Yuan, J. Zhang, Z. Huo, Y. Wang, N. Zhao, Y. Qin, K. Liu, R. Xi, G. Chen, H. Zhang, C. Tang, J. Yan, Q. Ge, H. Cheng, Y. Lu, L. Gao, *Nat. Commun.* **2023**, *14*, 7769.
[9] H. Kawakami, K. Nagatake, S. Ni, F. Nakamura, T. Takano, K. Murakami, I. Ohara, Y. Isano, R. Matsuda, H. Suwa, R. Higashi, M. Kanto, M. Saito, H. Fujita, T. Araki, S. Ozaki, K. Ueno, T. Horii, T. Fujie, H. Ota, *Adv. Mater. Technol.* **2024**, *9*, 2400487.
[10] T. Q. Trung, N.-E. Lee, *Adv. Mater.* **2017**, *29*, 1603167.
[11] S. Hou, C. Chen, L. Bai, J. Yu, Y. Cheng, W. Huang, *Small* **2024**, *20*, 2306749.
[12] M. Xu, J. Zhu, J. Xie, Y. Mao, W. Hu, *Small* **2024**, *20*, 2401481.
[13] Y. Song, R. Y. Tay, J. Li, C. Xu, J. Min, S. Sani, G. Kim, W. Heng, I. Kim, W. Gao, *Sci. Adv.* **2023**, *9*, 6492.
[14] Z. Wang, J. Zhu, *Small* **2024**, *20*, 2311012.
[15] N. Ochirkhuyag, Y. Nishitai, S. Mizuguchi, Y. Isano, S. Ni, K. Murakami, M. Shimamura, H. Iida, K. Ueno, H. Ota, *ACS Appl. Mater. Interfaces* **2022**, *14*, 48123.
[16] R. Yu, S. Feng, Q. Sun, H. Xu, Q. Jiang, J. Guo, B. Dai, D. Cui, K. Wang, *J. Nanobiotechnol.* **2024**, *22*, 669.
[17] Y. Yu, J. Nassar, C. Xu, J. Min, Y. Yang, A. Dai, R. Doshi, A. Huang, Y. Song, R. Gehlhar, A. D. Ames, *Sci. Robot.* **2020**, *5*, 7946.
[18] N. Xu, J. Han, J. Yang, Y. Wang, Y. Xiong, Z. L. Wang, Q. Sun, *Nano Energy* **2025**, *142*, 111153.
[19] S. Kim, S. Park, J. Choi, W. Hwang, S. Kim, I. S. Choi, H. Yi, R. Kwak, *Nat. Commun.* **2022**, *13*, 6705.
[20] Z. Cao, Y. Xu, S. Yu, Z. Huang, Y. Hu, W. Lin, H. Wang, Y. Luo, Y. Zheng, Z. Chen, Q. Liao, X. Liao, *Adv. Funct. Mater.* **2024**, *35*, 2412649.
[21] C. Liu, J. Yang, Z. Lu, C. Chen, J. Wang, D. Xu, X. Li, *Sensors* **2023**, *23*, 9737.
[22] R. Matsuda, Y. Isano, K. Ueno, H. Ota, *APL Bioeng.* **2023**, *7*, 016108.
[23] K. Yamagishi, W. Zhou, T. Ching, S. Ying Huang, M. Hashimoto, K. Yamagishi, T. Ching, M. Hashimoto, W. Zhou, S. Y. Huang, *Adv. Mater.* **2021**, *33*, 2008062.
[24] T. Sato, S. Watanabe, R. Takahashi, W. Yukita, T. Yokota, T. Someya, Y. Kawahara, E. Iwase, J. Kurumida, *Proceedings of the IEEE International Conference on Micro Electro Mechanical Systems (MEMS)*, Institute of Electrical and Electronics Engineers Inc, Taiwan, Province of China **2025**, 181–184.
[25] R. Lin, H. J. Kim, S. Achavananthadith, Z. Xiong, J. K. W. Lee, Y. L. Kong, J. S. Ho, *Nat. Commun.* **2022**, *13*, 2190.
[26] S. Kim, S. Choi, E. Oh, J. Byun, H. Kim, B. Lee, S. Lee, Y. Hong, *Sci. Rep.* **2016**, *6*.
[27] J. Vaicekauskaite, P. Mazurek, S. Vudayagiri, A. L. Skov, *J. Mater. Chem. C Mater.* **2020**, *8*, 1273.
[28] Z. Wang, A. A. Volinsky, N. D. Gallant, *J. Appl. Polym. Sci.* **2014**, *131*.
[29] G. Yun, S. Y. Tang, S. Sun, D. Yuan, Q. Zhao, L. Deng, S. Yan, Du, M. D. Dickey, W. Li, *Nat. Commun.* **2019**, *10*, 1.
[30] G. Yun, S. Y. Tang, Q. Zhao, Y. Zhang, H. Lu, D. Yuan, S. Sun, L. Deng, M. D. Dickey, W. Li, *Matter* **2020**, *3*, 824.
[31] W. Hong, C. Jiang, M. Qin, Z. Song, P. Ji, L. Wang, K. Tu, L. Lu, Z. Guo, B. Yang, X. Wang, J. Liu, *Sci. Adv.* **2021**, *7*, 4273.
[32] M. Stevens, G. Yun, T. Hasan, *Adv. Funct. Mater.* **2024**, *34*, 2309347.
[33] A. M. M. R. Persson, E. Andreassen, *Polymers* **2022**, *60*, 1642.
[34] C. Beutier, A. Serghei, P. Cassagnau, P. Heuillet, B. Cantaloube, N. Selles, I. Morfin, G. Sudre, L. David, *Polymer* **2022**, *254*, 125077.
[35] S. H. Jeong, K. Hjort, Z. Wu, *Sci. Rep.* **2015**, *5*, 1.
[36] H. A. Wheeler, *Proc. Inst. Radio Eng.* **1928**, *16*, 1398.
[37] S. Chae, W. Jin Choi, I. Fotev, E. Bittrich, P. Uhlmann, M. Schubert, D. Makarov, J. Wagner, A. Pashkin, A. Fery, *Adv. Mater.* **2021**, *33*, 2104769.
[38] W. K. Min, C. Won, D. H. Kim, S. Lee, J. Chung, S. Cho, T. Lee, H. J. Kim, *Adv. Mater.* **2023**, *35*, 2303556.
[39] W.-J. Song, M. Kong, S. Cho, S. Lee, J. Kwon, H. Bin Son, J. Hyuk Song, D.-G. Lee, G. Song, S.-Y. Lee, S. Jung, S. Park, U. Jeong, W. Song, S. Lee, H. B. Son, S. Park, M. Kong, U. Jeong, S. Cho, J. H. Song, J. Kwon, D. Lee, G. Song, S. Lee, S. Jung, *Adv. Funct. Mater.* **2020**, *30*, 2003608.
[40] X. Lin, Z. Feng, Y. Xiong, W. Sun, W. Yao, Y. Wei, Z. L. Wang, Q. Sun, *Int. J. Extrem. Manuf.* **2024**, *6*, 032011.